1-26-2009

Valley degeneracies in (111) silicon quantum wells

Neerav Kharche
Birck Nanotechnology Center, Network for Computational Nanotechnology, Purdue University, nkharche@purdue.edu

Seongmin Kim
Birck Nanotechnology Center, Network for Computational Nanotechnology, Purdue University, kim482@purdue.edu

Timothy B. Boykin
Department of Electrical and Computer Engineering, University of Alabama at Huntsville

Gerhard Klimeck
Birck Nanotechnology Center, Network for Computational Nanotechnology, Purdue University, gekco@purdue.edu

Valley degeneracies in (111) silicon quantum wells

Neerav Kharche,[1,a] Seongmin Kim,[1] Timothy B. Boykin,[2] and Gerhard Klimeck[3]
[1]*Birck Nanotechnology Center, Network for Computational Nanotechnology, Purdue University, West Lafayette, Indiana 47907-1285, USA*
[2]*Department of Electrical and Computer Engineering, University of Alabama at Huntsville, Huntsville, Alabama 35899, USA*
[3]*Birck Nanotechnology Center, Network for Computational Nanotechnology, Jet Propulsion Laboratory, California Institute of Technology, Pasadena, California 91109, USA*

(Received 3 November 2008; accepted 18 December 2008; published online 26 January 2009)

(111) silicon quantum wells have been studied extensively, yet no convincing explanation exists for the experimentally observed breaking of sixfold valley degeneracy into two- and fourfold degeneracies. Here, systematic $sp^3d^5s^*$ tight-binding and effective mass calculations are presented to show that a typical miscut modulates the energy levels, which leads to breaking of sixfold valley degeneracy into two lower and four raised valleys. An effective mass based valley-projection model is used to determine the directions of valley minima in tight-binding calculations of large supercells. Tight-binding calculations are in better agreement with experiments compared to effective mass calculations. © *2009 American Institute of Physics*. [DOI: 10.1063/1.3068499]

Silicon nanostructures exhibit a plethora of interesting physical phenomena due to the sixfold valley degeneracy of the bulk conduction band. Silicon devices are being pursued for spin based quantum computing[1] and spintronics[2] due to their scaling potential and integrability within the industrial nanoelectronic infrastructure. Relative energies and degeneracies of spin and valley states are critical for device operation in these novel computing architectures[1,2] and conventional metal-oxide-semiconductor field-effect transistors (MOSFETs) that often involve the formation of a two-dimensional electron gas (2DEG) at the semiconductor-insulator interface. Valley degeneracy of the 2DEG is highly dependent on the interface orientation. (100) Si quantum wells (QWs) show lower twofold and raised fourfold valley degeneracy, while (110) Si QWs show lower fourfold and raised twofold valley degeneracy. The origin of these valley degeneracies is well understood and the experimental observations are in agreement with the effective mass based theoretical predictions.[3]

Valley degeneracy in (111) Si QWs should be six according to standard effective mass theory. Experimental measurements on (111) Si/SiO_2 MOSFETs, however, show a conflicting valley degeneracy of two and four.[3–5] Recently two to four valley splitting has also been observed in magnetotransport measurements performed on hydrogen terminated (111) Si/vacuum FETs.[6] Previously proposed theory of local strain domains[4] cannot explain this splitting since the Si-vacuum interface is stress free. The splitting is also unlikely to be a many-body phenomenon.[7]

Careful imaging of the surface morphology shows the presence of monoatomic steps (miscut) on the (111) Si surface[6,8] as well as at the Si/SiO_2 interface in (111) Si MOSFETs.[8,9] Atomistic models such as tight binding are needed to accurately model the electronic structure of miscut QWs.[10] Through systematic tight-binding calculations of flat and miscut (111) Si QWs, we show that the surface miscut leads to the two to four degeneracy breaking and resolve the conflict between theory and experimental observations. To reduce the computational burden associated with searching the whole Brillouin zone for valley minima, an effective mass based valley-projection model[11] tailored to miscut (111) surfaces is used. Electronic structure calculations are performed using the general purpose NEMO-3D Code.[12]

Hydrogen terminated (111) Si surfaces as well as the (111) Si/SiO_2 interfaces have monatomic steps [Figs. 1(a) and 1(b)]. For simplicity, the steps are assumed to run perpendicular to the $[11\bar{2}]$ direction. This surface morphology can be implemented by repeating the rectangular unit cell of Fig. 1(c) in the miscut $[11\bar{2}]$ direction. The in-plane unit cell dimensions are $a_x=\sqrt{3/2}a_{Si}$ and $a_y=\sqrt{1/2}a_{Si}$, where a_{Si} is Si lattice constant.[13] The advantage of using a rectangular unit cell is twofold. First, the rectangular geometry simplifies the underlying mathematics and implementation of the periodic boundary conditions in the bandstructure calculation. Second, the surface miscut can be easily implemented by applying shifted boundary condition to the rectangular supercell.

The Brillouin zone and six degenerate valleys in the bandstructure of the hexagonal primitive unit cell of a flat (111) Si QW [Fig. 1(c)] are shown in Fig. 2(a). The two bulk valleys along the [001] direction are projected along the

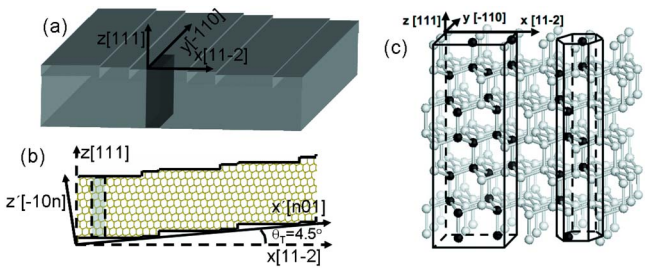

FIG. 1. (Color online) (a) Schematic of a miscut (111) QW. A rectangular unit cell is repeated in space to build the miscut QW. (b) Atomistic view of a unit cell of a 4.5° miscut (111) Si QW. The reduced symmetry along the direction perpendicular to steps results in a larger unit cell. The smallest repeated miscut QW unit cell along the $[11\bar{2}]$ direction has six steps. (c) Atomistic view of a flat (111) Si QW. The rectangular unit cell is larger than the hexagonal primitive unit cell.

[a]Electronic mail: nkharche@purdue.edu.

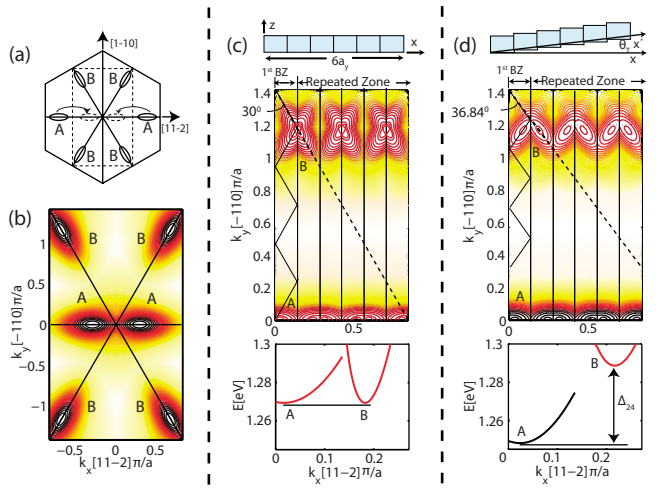

FIG. 2. (Color online) (a) Brillouin zone of the primitive unit cell of a flat (111) Si QW. Six degenerate valleys are shown. (b) Brillouin zone and bandstructure of a (111) Si QW plotted using the rectangular unit cell of Fig. 1(b). The bandstructure is folded as shown schematically in (a). (c) Bandstructure of a flat (111) Si QW in repeated zone scheme plotted using a supercell, which contains six small cells in the x-direction. The bandstructure of Fig. 1(b) is folded in the first Brillouin zone. A-type valleys along the k_x-direction and B-type valleys along the dotted lines are degenerate. (d) Bandstructure of a 13° miscut (111) Si QW in repeated zone scheme. A-type valleys along the k_x-direction are lower in energy than B-type valleys along the dotted line. In the flat QW the dotted line subtends an angle of 30° with the negative y-axis, while this angle is 36.84° in a miscut QW.

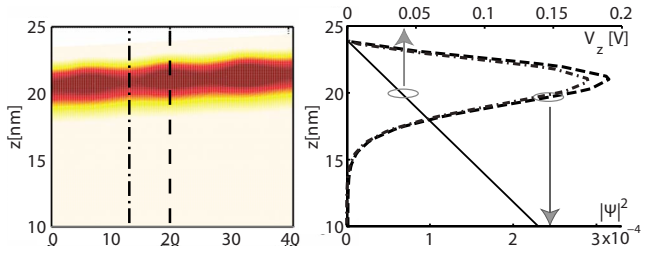

FIG. 3. (Color online) (a) A typical wave function of a 4.5° miscut (111) Si QW of Fig. 1(b) at the valley minimum. Thickness of the QW is 23 nm, however, only the near surface portion having appreciable wave function magnitude is shown. (b) Electrostatic potential and wave function cut along two dotted lines in (a). Confining potential due to constant electric field (10 MV/m) pulls the wave function to the surface. Surface steps modulate the wave function amplitude and modify energy levels, which give rise to the Δ_{2-4} splitting.

$[11\bar{2}]$ direction, while the remaining four bulk valleys along [100] and [010] are symmetrically projected in each of the four quadrants.[11] The two valleys along $[11\bar{2}]$ are labeled as A and remaining four valleys are labeled as B. The rectangular unit cell is larger than the hexagonal primitive unit cell [Fig. 1(c)]. The Brillouin zone of the rectangular unit cell in Fig. 1(b) is given by $\{(k_x,k_y):-\sqrt{2/3}\pi/a_{\mathrm{Si}}\leq k_x \leq \sqrt{2/3}\pi/a_{\mathrm{Si}},-\sqrt{2}\pi/a_{\mathrm{Si}}\leq k_y\leq\sqrt{2}\pi/a_{\mathrm{Si}}\}$. It is smaller than the hexagonal Brillouin zone in Fig. 1(a) and 2A type valleys are folded.

The miscut surface morphology can be conveniently implemented by extending the rectangular unit cell in one direction [Figs. 1(b) and 1(c)]. The unit cell shown in Fig. 1(b) has a miscut angle of 4.5°. In the (x,y,z) coordinate system in Fig. 1(a), the surface normal of this QW is along the $[\bar{1}0n]$ direction. This direction is related to the miscut angle by $\theta_T=\tan^{-1}(a_z/na_x)$, where $a_x=\sqrt{3/2}a_{\mathrm{Si}}$ and $a_z=\sqrt{3}a_{\mathrm{Si}}$.

Typical miscuts range from 0.1° to 8°. Before going to the experimental 0.2° miscut,[6] we illustrate the essential physics and reduce the computational burden significantly by studying the effect the miscut of 13°, which can be investigated in a system extending six unit cells along the miscut direction and has a smaller supercell compared to 0.2° miscut. These unit cells are schematically shown along with energy contours of their lowest conduction bands in Figs. 2(c) and 2(d). Only the positive quadrant is shown. The flat QW supercell of Fig. 2(c) is six times longer in the x-direction compared to the rectangular unit cell used to plot the bandstructure in Fig. 2(b) resulting in zone folding of this supercell to 1/6th. In the first Brillouin zone A-type valleys lie along the k_x-direction and the B-type valleys lie along the solid zigzag line. In the repeated-zone scheme the bandstructures along the solid zigzag line is the same as that along the dotted straight line. The bands corresponding to A- and B-type valleys clearly show that in a flat (111) Si QW, both valleys are degenerate while in a miscut QW two A-type valleys have lower energy compared to four B-type valleys [Fig. 3(d)]. This degeneracy breaking is the effect of different confinement effective masses of A- and B-type valleys in a miscut QW.

Experimentally relevant QWs have typical miscuts ranging from 0.1° to 8°. As the miscut angle becomes smaller the size of the unit cell increases. For example, the unit cell of 23 nm thick 13° miscut QW contains 2100 atoms, while a 0.2° miscut QW requires 119 100 atoms. An effective mass theory can be used to determine the directions of valley minima thereby reducing the computational burden associated with searching the whole Brillouin zone. Here we outline the valley projection model[11] as applied to determine the directions of valley minima of miscut (111) Si QWs.

Consider the miscut QW unit cell of Fig. 1(c), the rotation matrix R from bulk valley coordinate system to (x',y,z') coordinate system is given by

$$R=\frac{1}{\sqrt{n^2+1}}\begin{bmatrix} n & 0 & 1\\ 0 & 1 & 0\\ -1 & 0 & n\end{bmatrix}\begin{bmatrix} 1/\sqrt{6} & 1/\sqrt{6} & -\sqrt{2/3}\\ -1/\sqrt{2} & 1/\sqrt{2} & 0\\ 1/\sqrt{3} & 1/\sqrt{3} & 1/\sqrt{3}\end{bmatrix}. \quad (1)$$

In the effective mass formalism the subbands of this QW are given by[10]

$$E_i(k_{x'},k_y)=E_i^0+\tfrac{1}{2}\hbar^2\left[\left(w_{x'x'}-\frac{w_{x'z'}^2}{w_{z'z'}}\right)k_{x'}^2+2\left(w_{x'y}-\frac{w_{x'z'}w_{yz}}{w_{z'z'}}\right)k_{x'}k_y+\left(w_{yy}-\frac{w_{yz'}^2}{w_{z'z'}}\right)k_y^2\right], \quad (2)$$

where the reciprocal effective mass matrix $[W]$ is given by

$$[W]_{ij}=\sum_\alpha R_{i\alpha}R_{j\alpha}[M_0]^{-1}_{\alpha\alpha},\quad i,j,\alpha\in\{x',y,z'\}. \quad (3)$$

Here $[M_0]$ is the effective mass matrix in the bulk valley coordinate system. The position of the subband minimum E_i^0 is determined by the confinement effective mass $m_{z'}=1/w_{z'z'}$ and the confinement potential in the direction per-

pendicular to the QW surface. In this formalism two *A*-type valleys, which lie along the [100] direction are projected along $k_{x'}$, while the remaining four *B*-type valleys are projected along the directions, which subtend angles $\pm\varphi$ with $\pm k_y$ axis. The angle φ can be determined by rotating the coordinate system $(k_{x'}, k_y)$ such that the cross term in Eq. (2) vanishes. This angle is given by $\varphi=(1/2)\tan^{-1}[c/(a-b)]$ where a, b, and c denote coefficients of terms $k_{x'}^2$, k_y^2, and $k_{x'}k_y$, respectively. One of these four directions that lie in the positive quadrant is shown for flat and miscut QWs in Fig. 2.

While in a flat (111) QW confinement effective masses $m_{z'}$ are the same for *A*- and *B*-type valleys, a miscut alters these masses such that $m_A > m_B$ resulting in a broken degeneracy of lower twofold and raised fourfold. Although the effective mass theory can explain the origin of Δ_{2-4} splitting, more sophisticated methods such as tight binding are needed to accurately model the effect of monoatomic surface steps on the electronic structure. The Δ_{2-4} splitting increases with the miscut angle due to increasing difference between confinement effective masses of *A*- and *B*-type valleys. Both effective mass and tight-binding models show this trend; the effective mass model, however, gives smaller splitting compared to the tight-binding model. As shown in Fig. 3 the step morphology of the QW surface modulates the wave function, which in turn influence energy levels to give rise to Δ_{2-4} splitting.

A 0.2° miscut resembles closely to that of the experiment.[6] The unit cell of a QW of this miscut is $L_x = 264.07$ and $L_y = 0.38$ nm long in the *x*- and *y*-directions, respectively. A constant *z*-directed electric field of 10 MV/m, which corresponds to the electron density of 6.5×10^{11} cm^{-2}, is assumed.[6] To avoid any truncation effects of electronic domain on eigenvalues, a QW thickness of $L_z = 23$ nm is simulated. This is the smallest unit cell, which can be repeated in the *xy*-plane to generate a 23 nm thick 0.2° miscut QW. This unit cell contains around 0.1×10^6 atoms, which makes it computationally expensive to search the whole two-dimensional Brillouin zone for valley minima. To reduce the computational burden, the valley-projection method described above is used to identify the directions of valley minima. The valley minima of *A*-type valleys occur along the k_x-direction, while valley minima of *B*-type valleys occur at an angle $\varphi = \pm 30.13°$ to k_y axis. The confinement effective masses m_z for *A*- and *B*-type valleys are $0.2608m_0$ and $0.2593m_0$ (where m_0 is the mass of the free electron), respectively. The Δ_{2-4} valley splitting in a 0.2° miscut QW calculated using an effective mass and the $sp^3d^5s^*$ tight-binding models are 1.25 (108 μeV) and 3.98 K (343 μeV), respectively. An analytical formula for energy levels in triangular potential wells is used to estimate the splitting in the effective mass model.[11] The splitting reported from the temperature dependence of the longitudinal resistance[6] is 7 K (604 μeV), which shows that the tight-binding calculation matches closer to experiments compared to the effective mass calculation.

In conclusion, the miscut morphology of the (111) Si surface is shown to be the origin of breaking of sixfold valley degeneracy into lower two and raised fourfold valley degeneracies. Atomistic basis representation such as tight binding is needed to capture the effect of wave function modulation at monoatomic steps on the electronic structure. Compared to effective mass the tight-binding calculations are found to match closer to experimentally measured Δ_{2-4} splitting. Additional surface phenomena could be responsible for enhanced Δ_{2-4} splitting reported in experiments.[6]

This work was supported by Semiconductor Research Corporation and the Army Research Office. The work described in this publication was carried out in part at the Jet Propulsion Laboratory, California Institute of Technology under a contract with the National Aeronautics and Space Administration and Jet Propulsion Laboratory. nanoHUB.org computational resources operated by the Network for Computational Nanotechnology, funded by the National Science Foundation were used.

[1] B. E. Kane, Nature (London) **393**, 133 (1998); D. Loss and D. P. DiVincenzo, Phys. Rev. A **57**, 120 (1998).
[2] I. Appelbaum, B. Huang, and D. J. Monsma, Nature (London) **447**, 295 (2007).
[3] T. Ando, A. B. Fowler, and F. Stern, Rev. Mod. Phys. **54**, 437 (1982).
[4] D. C. Tsui and G. Kaminsky, Solid State Commun. **20**, 93 (1976).
[5] T. Cole and B. D. McCombe, Phys. Rev. B **29**, 3180 (1984).
[6] K. Eng, R. N. McFarland, and B. E. Kane, Phys. Rev. Lett. **99**, 016801 (2007).
[7] M. J. Kelly and L. M. Falicov, Phys. Rev. Lett. **37**, 1021 (1976); E. H. Hwang and S. D. Sarma, *ibid.* **75**, 073301 (2007).
[8] H. Watanabe, K. Fujita, and M. Ichikawa, Surf. Sci. **385**, L952 (1997).
[9] H. S. Momose, T. Ohguro, S.-I. Nakamura, Y. Toyoshima, H. Ishiuchi, and H. Iwai, IEEE Trans. Electron Devices **49**, 1597 (2002).
[10] N. Kharche, M. Prada, T. B.Boykin, and G. Klimeck, Appl. Phys. Lett. **90**, 092109 (2007).
[11] F. Stern and W. E. Howard, Phys. Rev. **163**, 816 (1967).
[12] G. Klimeck, S. Ahmed, H. Bae, N. Kharche, R. Rahman, S. Clark, B. Haley, S. Lee, M. Naumov, H. Ryu, F. Saied, M. Prada, M. Korkusinski, and T. B. Boykin, IEEE Trans. Electron Devices **54**, 2079 (2007).
[13] T. B. Boykin, N. Kharche, and G. Klimeck, Physica E (Amsterdam) **41**, 490 (2009).